NASA CONTRACTOR REPORT

NASA CR-402

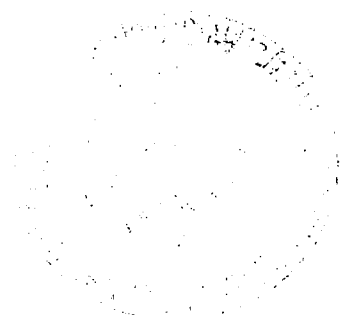NASA CR-40

THERMAL PROPERTIES OF SOLID AND POROUS TUNGSTEN AT TEMPERATURES TO 5000° F

by S. L. Israel, T. D. Hawkins, and S. C. Hyman

NATIONAL AERONAUTICS AND SPACE ADMINISTRATION • WASHINGTON, D. C. • MARCH 1966

THERMAL PROPERTIES OF SOLID AND POROUS

TUNGSTEN AT TEMPERATURES TO 5000° F

By S. L. Israel, T. D. Hawkins, and S. C. Hyman

Distribution of this report is provided in the interest of information exchange. Responsibility for the contents resides in the author or organization that prepared it.

FOREWORD

To experimentally determine the thermal conductivity of hydrogen at high temperatures by the method reported in NASA CR-403 the thermal properties of both the porous and solid tungsten test specimens must be accurately known. These properties are the spectral emittance, the total normal emittance, the total hemispherical emittance, and the thermal conductivity for solid and porous tungsten. The experimental data used to determine these properties are recorded in NASA CR-54429. This work was completed under the technical management of Maynard F. Taylor, Lewis Research Center, Cleveland, Ohio.

TABLE OF CONTENTS

1. SUMMARY

An experimental program was conducted to determine the thermal conductivity of solid and porous tungsten at temperatures up to 5000°F. The method used in this program was to measure the temperature distribution on the top surface of a cylindrical specimen heated in a vacuum by r-f induction currents and radiating freely. The thermal conductivity was determined by equating the axial heat flux within the specimen to the radiation flux at the center of the top surface.

A digital computer program was used to relate the axial heat flux within the specimen to the temperature distribution on the top surface. The program calculates the temperature distribution in the specimen from an assumed finite depth of induction heating at the outer cylindrical surface and radiation boundary conditions. The results of this computer study were used to determine a proportionality factor that permits calculating the axial temperature gradient and heat flux at the center of the top surface from the measured top surface temperature distribution.

The thermal conductivity of solid tungsten was found to vary from 76 Btu/hr-ft-°F at 3000°F to 66 Btu/hr-ft-°F at 5000°F. These values are in reasonable agreement with recently published data. The thermal conductivities calculated for porous tungsten specimens (0.42 to 0.55 porosity) are 10 to 15% of the solid thermal conductivity. The variation between specimens is attributed to the differences in the degree of sintering during fabrication. Thermal conductivity data for the porous specimens vary little with temperature, indicating that internal

radiation within the specimen had no significant effect on the effective thermal conductivity.

Spectral emittances, derived from optical pyrometer measurements, were obtained for the solid and porous tungsten specimens. The values for solid tungsten vary from 0.46 at 2000°F to 0.38 at 5000°F. The porous tungsten emittances (0.65 at 4000°F) are significantly higher than the solid values because of the rough texture of the surface.

Total normal emittances were measured using a total radiation pyrometer. The solid tungsten emittances vary between 0.2 and 0.3 for temperatures of 2500 to 4300°F. These values are in good agreement with published data. The total normal emittance for porous tungsten is approximately 0.59.

The total hemispherical emittances were measured using a transient technique. This method equates the sensible heat loss of the specimen to its radiation heat losses. The value of total hemispherical emittances for the solid tungsten is approximately 0.335. The value for the porous tungsten is 0.595.

2. INTRODUCTION

With the advent of high temperature systems, there has been an increasing inter-
est in refractory metals such as tungsten, which has a melting temperature
greater than 6000°F. A considerable amount of information on the thermal prop-
erties of tungsten was generated in the early part of this century. More recently,
investigators have been examining its application in rocket nozzles and high per-
formance reactors for nuclear rockets.

The thermal conductivity of solid tungsten has been measured by a number of
investigators. Results, however, have not been in good agreement. Values rang-
ing from 100 to 30 Btu/hr-ft-°F have been reported at a temperature of 3000°F.
A recent compilation of data[1] on tungsten indicated that 50 to 60 Btu/hr-ft-°F was
a reasonable value for the thermal conductivity at this temperature. The interest
in the thermal conductivity of tungsten in this program is its use in an experimen-
tal investigation of hydrogen thermal conductivity.[2] This program uses hydrogen
filled, porous tungsten specimens, and requires a knowledge of solid tungsten
thermal conductivity as well as the thermal conductivity of the porous specimens
in vacuum to obtain gas thermal conductivity values.

The technique used in these thermal conductivity experiments was developed by
Hoch,[3] and requires measurement of the temperature distribution on the top circu-
lar surface of a cylindrical specimen heated by r-f induction current. By means
of numerical analysis, the measured temperature distribution across the top sur-

face of the specimen is related to the axial heat flux within the specimen. This heat flux is then equated to the radiation heat flux leaving the surface of the specimen. Since the heat flux within the specimen is proportional to the thermal conductivity, this property can be determined from the measured temperatures.

Spectral emittances for the solid and porous tungsten specimens are measured with an optical pyrometer (wave length 0.65 μ) using a black body hole to establish the true temperatures. The spectral emittance, which is based on the radiant energy over a small wave length band at 0.65 μ leaving a surface in the normal direction, is used to obtain true temperatures from the optical pyrometer data.

The total normal emittance is based on the radiant energy for all wave lengths leaving the specimen surface in the normal direction. It is measured with a total radiation pyrometer which is calibrated with a black body.

The total hemispherical emittances for the solid and porous tungsten specimens is measured by a transient technique also proposed by Hoch.[4] The method is based on relating the radiation heat loss from the specimen to the sensible heat loss. The total hemispherical emittance refers to the radiant energy leaving a surface for all wave lengths and viewing angles and is used in the thermal conductivity determinations.

The results of all these property measurements are used in a concurrent program to measure hydrogen thermal conductivity.

3. TECHNICAL APPROACH

3.1 THEORY

The experimental approach used in determining thermal conductivity at elevated temperatures was to measure the temperature distribution on the upper circular surface of a cylindrical specimen heated by r-f induction currents. The arrangement is shown in Fig. 1. The heating of the specimen, caused by the induced currents, is assumed to be uniform in the axial direction and its magnitude decreases exponentially with increased distance from the outer cylindrical surface. It is estimated from calculations that the depth of heating in the solid tungsten specimens is 0.030 in. The depth of heating in the porous tungsten specimens is estimated from temperature measurements to be 0.2 in. The increased depth of heating in the porous specimens results from a greater electrical resistance and decreased magnetic permeability.

Heat loss from the specimen is by thermal radiation from the outer surfaces of the specimen to the cooled walls of the test chamber. Since heat is generated only in a thin outer cylindrical portion of the specimen, radial and axial temperature gradients are established to conduct heat to the radiating end faces of the specimen. Thus, the experimental system provides the conditions needed for thermal conductivity determinations, i.e., a means of establishing desired specimen temperatures, a means of measuring surface temperature distribution, and a means of measuring surface heat flux (radiation).
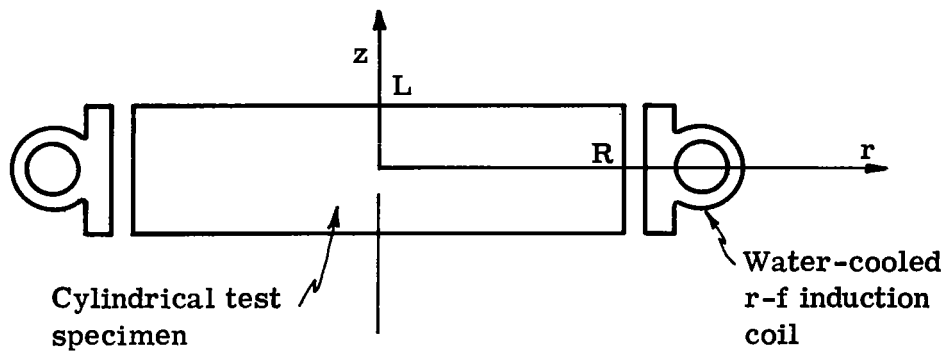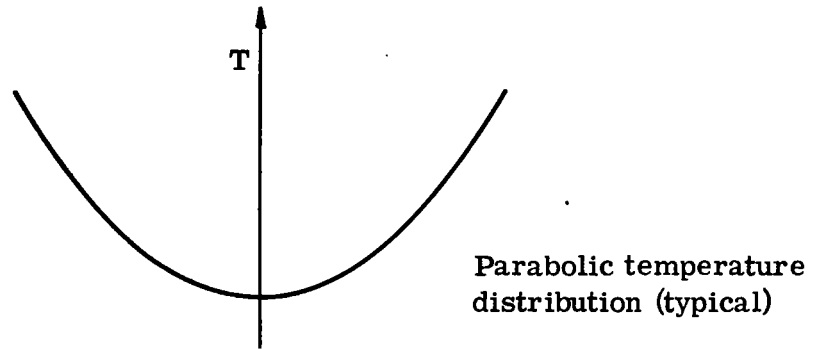
Fig. 1 — Specimen Arrangement

The thermal conductivity of the specimen is determined by equating the axial heat flux within the specimen at the center of the top surface to the radiation heat flux at that point.

$$-k \left. \frac{\partial T}{\partial z} \right|_{0,L} = \epsilon_T \sigma T_{0,L}^4 \qquad (1)$$

The radiation heat flux given by the term on the right-hand side of Eq. 1 is calculated from the measured temperature at the center of the top surface of the specimen and the total hemispherical emittance which is experimentally determined. The axial temperature gradient on the left side can not be measured directly, but must be determined from the measured radial temperature profile on the top circular surface and a knowledge of the temperature distribution within the specimen.

The temperature distribution in a short cylindrical specimen is the solution to Poisson's equation,

$$\frac{\partial^2 T}{\partial r^2} + \frac{1}{r} \frac{\partial T}{\partial r} + \frac{\partial^2 T}{\partial z^2} + \frac{Q_0}{k} = 0$$

with radiation boundary conditions. A closed form solution to a simplified version of the above boundary value problem was obtained by Hoch,[3] who first proposed this method for determining thermal conductivity. The source term, Q_0, was eliminated since heating occurred in a very thin layer near the cylindrical surface of the specimen. In addition, experimentally observed temperature distributions were used as boundary conditions instead of the nonlinear radiation conditions which are intractable for an analytical solution. A parabolic temperature distribution was used for the circular end faces and a uniform temperature was assumed on the outer cylindrical surface. A later analysis by Hoch[3] used a linear temperature gradient on the outer cylindrical surface (peak temperature at the midplane) equal to 10% of the radial difference at the top surface to account for

uncertainties in temperature measurements on the outer surface. Results showed that the axial temperature gradient at the center of the top surface can be related to the radial temperature difference across the upper circular surface by

$$-\left.\frac{\partial T}{\partial z}\right|_{0,L} = S_0 \frac{T_{R,L} - T_{0,L}}{R} \tag{2}$$

where S_0 is a proportionality factor that is determined by the geometry of the specimen. The proportionality factor was found to be insensitive to the outer boundary conditions if the aspect ratio (L/R) of the specimen was less than about 0.3.

3.2 PRESENT THEORETICAL APPROACH

The present work with porous tungsten shows a finite depth of heating in these specimens and indicates that specimens with aspect ratios larger than 0.3 would be desirable. Because Hoch's analysis[3] is not applicable to these conditions, a computer program was written to calculate the two-dimensional axisymmetric temperatures. The assumptions used were:

1. Uniform thermal conductivity.
2. Radiation heat losses from all boundary surfaces with uniform emittance.
3. Heat generation in the outer cylindrical layer is axially uniform and decreases linearly with penetration from the outer cylindrical surface. A 0.030-in. depth of heating was used for the solid tungsten and a 0.2-in. depth was used for the porous tungsten.

Between 20 and 30 radial nodes and 10 to 15 axial nodes were included in the finite difference network. The method of overrelaxation was used to obtain the solution based on a convergence criterion of a deviation less than 0.05°F at each node. A description of the equations used in the code is given in Appendix A.

Temperature distributions were calculated for different specimen geometries at various temperature levels. A thermal conductivity of 51.2 Btu/hr-ft-°F and total emittances between 0.2 and 0.32 were used for the solid tungsten. For porous tungsten, an emittance of 0.37 and a thermal conductivity of 6 Btu/hr-ft-°F was used. Subsequent work indicated that the actual values of thermal conductivity and emittances are higher than those used, but the ratio of radiation to conduction is the same. Therefore, the calculated temperature distributions obtained in this parametric study are considered applicable to the specimens used in the thermal conductivity measurements.

Typical temperature distributions calculated for solid and porous tungsten specimens of the same geometry are shown in Fig. 2. The two significant features of these curves are:

1. The temperature distribution on the upper circular surface in the zero heat generation region is parabolic. This confirms the experimental observations.

2. There is an appreciable temperature gradient on the outer cylindrical surface.

The first result shows that the temperature distribution on the circular faces is not affected by the depth of heating when the zero heat generation region is considered alone. Consequently, the solid and porous tungsten specimens can be treated in the same fashion. The second result indicates that proportionality factors, based on Hoch's assumed boundary conditions on the cylindrical surface, should be modified especially for specimens with larger aspect ratios where the temperature gradient on the outer surface is appreciable.

Proportionality factors were derived from the computer calculated temperature distributions using the following expression:
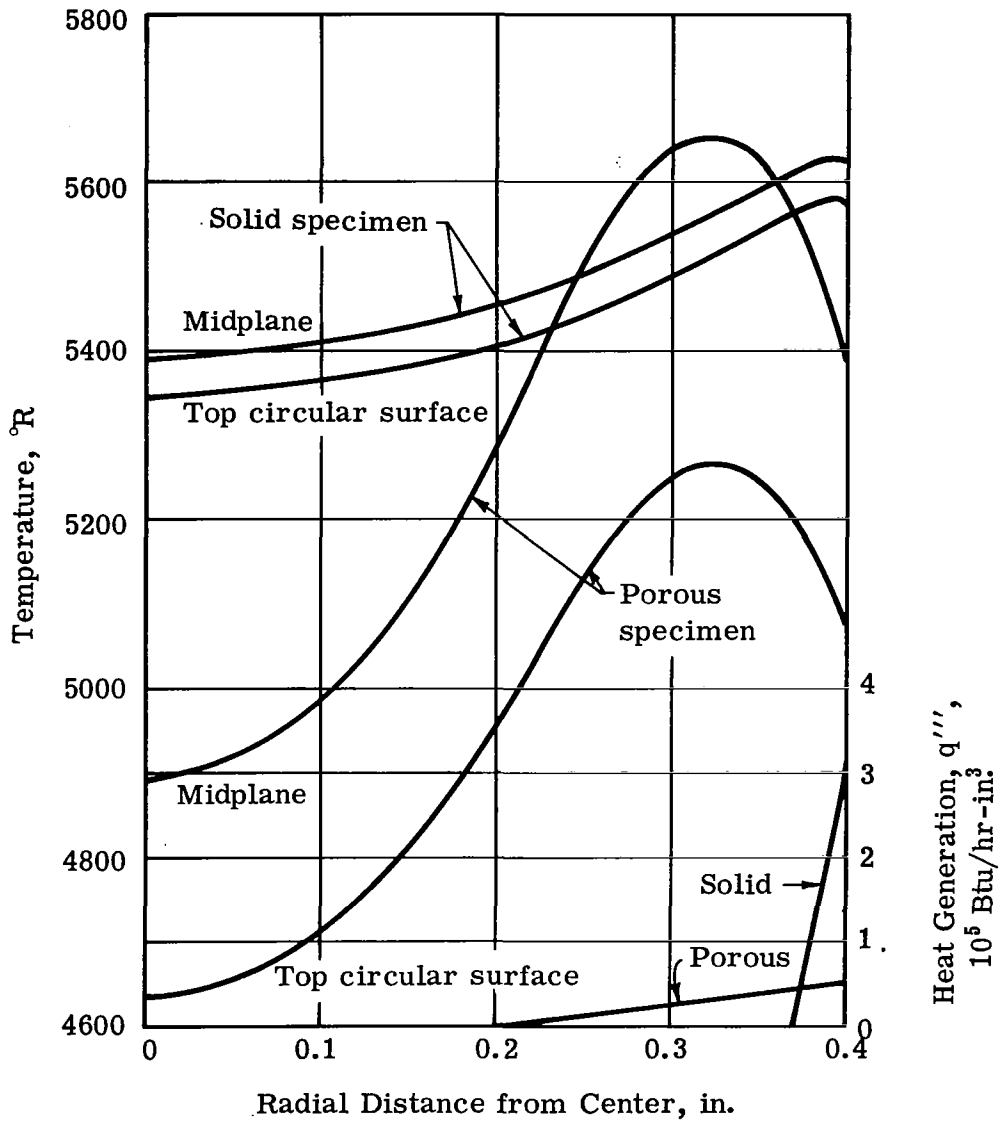
Fig. 2 — Typical Temperature Distributions in Solid and Porous Tungsten Specimens

	Diameter, in.	Height, in.	k, Btu/hr-ft-°F	ϵ_T
Solid	0.8	0.24	51.2	0.318
Porous	0.8	0.24	6	0.37

$$S_0 = \frac{\epsilon_T \sigma T_0^4}{\frac{k}{R}(T_{R,L} - T_{0,L})}$$

which is obtained by combining Eqs. 1 and 2. The calculated proportionality factors for solid and porous tungsten specimens are shown in Fig. 3. The scatter in the points derived from the parametric study are caused by inaccuracies in the numerical solution. At small aspect ratios, the computer results are in good agreement with Hoch's values obtained from both boundary value problems. At large aspect ratios, the computer calculated proportionality factors remain a linear function of the aspect ratio while Hoch's values tend to become independent of the geometry. This difference is attributed to the different boundary conditions used in obtaining the solutions. It may be observed from Fig. 3 that when the restriction of uniform cylindrical surface temperature is relaxed in Hoch's second analysis (dashed line in Fig. 3), the values approach those of the numerical solution.

Combining Eqs. 1 and 2, an expression for the thermal conductivity of a specimen is obtained.

$$k = \frac{\epsilon_T \sigma T_{0,L}^4}{\frac{S_0}{R}(T_{R,L} - T_{0,L})} \tag{3}$$

Thermal conductivities may be determined from Eq. 3 using measured temperatures on the upper circular surface, the proportionality constant for the specimen geometry, and the total hemispherical emittance which is experimentally determined.

3.3 EXPERIMENTAL APPARATUS

The experimental apparatus, shown schematically in Fig. 4, consists of an r-f power supply, test chamber, and atmosphere control and temperature measure-
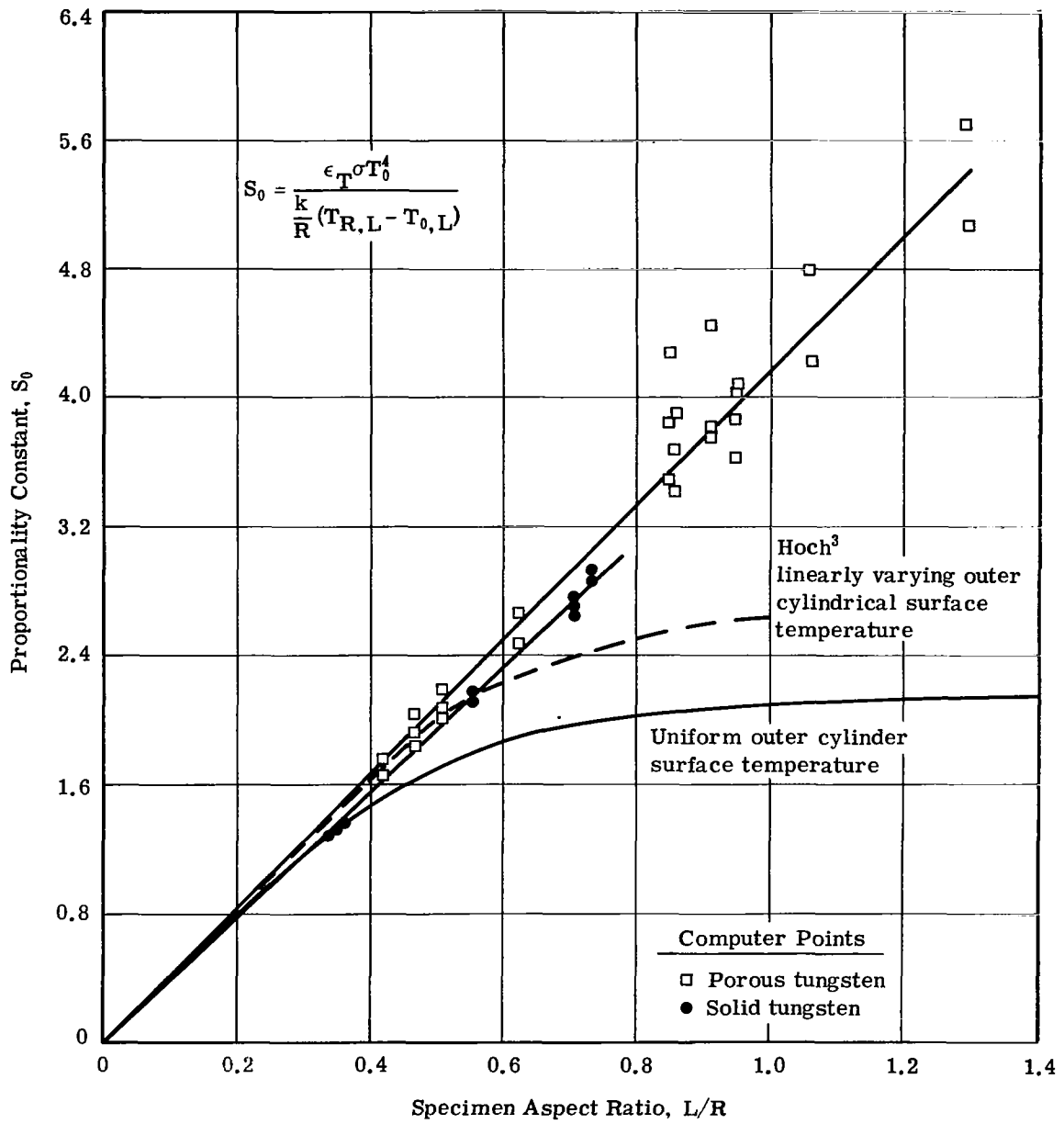
$$S_0 = \frac{\epsilon_T \sigma T_0^4}{\frac{k}{R}(T_{R,L} - T_{0,L})}$$

Hoch[3]
linearly varying outer
cylindrical surface
temperature

Uniform outer cylinder
surface temperature

Computer Points

□ Porous tungsten
● Solid tungsten

Proportionality Constant, S_0

Specimen Aspect Ratio, L/R

Fig. 3 — Proportionality Constant

MIRROR FOR
HORIZ. VIEWING

QUARTZ
VIEW PORT

TO VENT THRU
FLAME ARRESTOR

COOLING COILS

FI-1

STAINLESS ST'L.
BELL JAR

HIGH FREQUENCY
INDUCTION COIL
(GENERATOR NOT SHOWN)

TEST SPECIMEN

RD-1

QUARTZ
VIEW PORT

V-5

BACK
PRESS.
RESTR'N.

PR-1

PRESS.
REG.

V-1

PG-1
PRESS GAGE

V-3

GAS
PURIFIER

DRYING
COLUMN

ISOLATION
VALVES

V-4 VAC.
GAGE

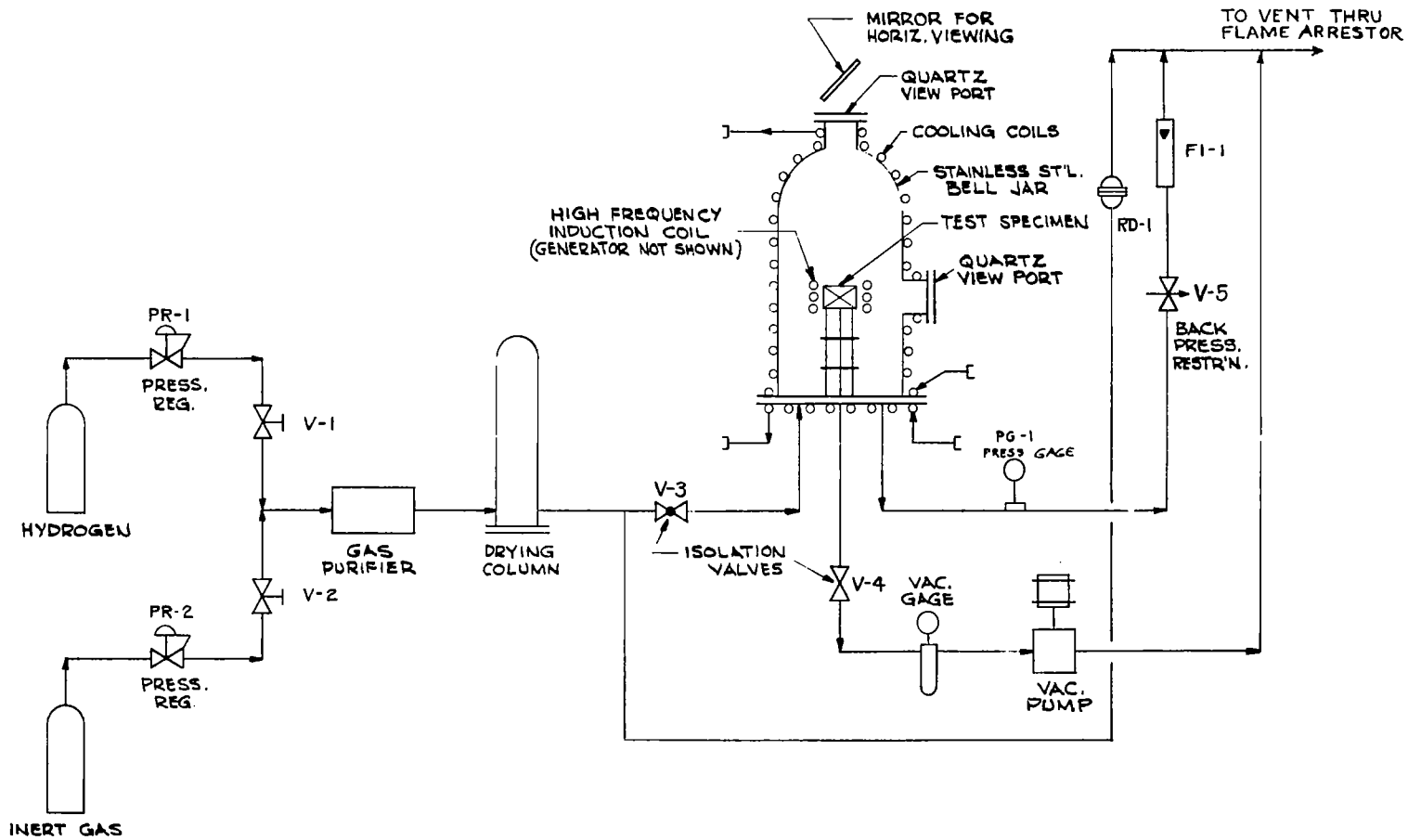HYDROGEN

PR-2

PRESS.
REG.

V-2

VAC.
PUMP

INERT GAS

Fig. 4 — Thermal Conductivity Apparatus — Schematic

ment instrumentation. The high-frequency power supply is capable of 20-kw power at frequencies from 300 to 450 kc. The frequency, which is determined by tuning requirements, is approximately 300 kc for this application. The bell jar table, which contains a step-down transformer, is connected to the converter by water-cooled leads. The step-down transformer improves the power transfer to the specimen, and, by reducing the voltage across the load coil, minimizes gas ionization in the test chamber. The bell jar table has a coaxial lead-through which connects the step-down transformer to the load coil inside the test chamber.

The test chamber, a stainless steel bell jar, is bolted to the base plate on the bell jar table. Two viewing ports are provided in the bell jar to permit observation of the upper circular surface and the vertical cylindrical surface of the test specimen as shown in Fig. 4. Quartz windows, 1-in. thick, are used in the viewing ports. A front surfaced mirror, attached to the upper viewing port, facilitates making temperature measurements on the upper circular surface of the specimen.

The specimen is supported within the bell jar by a tripod fabricated from pointed tungsten rods. It is centered in a single turn load coil as shown in Fig. 1. The load coils are the same height as the specimens and have a radial clearance of 0.1 in.

Temperature measurements are made with a micro-optical pyrometer. Measurements are made by matching the brightness of the pyrometer filament to the brightness of the specimen at a wave length of 0.65 microns. The pyrometer is attached to a vertically mounted circular milling table that permits positioning the disappearing filament in the pyrometer along two mutually perpendicular diameters of the upper circular surface of the specimen.

A total radiation pyrometer head and single-pen millivolt recorder provide for measuring total emittance. The pyrometer head is positioned above the upper

view port and is focused on the specimen's top surface with a target diameter of 0.2 in.

The test chamber can be pressurized with gas to 150 psia, or it can be evacuated with a mechanical vacuum pump to 5 microns Hg. A Bourdon tube-type pressure gauge and a thermocouple-type vacuum gauge are used to measure the test chamber pressure.

4. THERMAL CONDUCTIVITY MEASUREMENTS

Thermal conductivity measurements were made with solid and porous tungsten specimens. The four solid and five porous specimens used in these tests are listed in Table 1. The specimens were certified by the supplier to have a purity greater than 99.8% except for porous specimen P1 which was a trial specimen of unknown purity. Porous specimens P2 to P5 had porosities between 42 and 46% and specimen P1 had a porosity of 55%.

TABLE 1 — TEST SPECIMENS

	Diameter, in.	Height, in.
Solid Tungsten Specimens		
S1	1.52	0.502
S2	1.006	0.504
S3	1.0066	0.356
S4	0.804	0.284
S5	0.62	0.208
Porous Tungsten Specimens		
P1	1.52	0.538
P2	1.45	0.507
P3	0.975	0.379
P4	1.03	0.302
P5	0.80	0.25

The specimen dimensions shown in Table 1 were based on the results of the computer study of the temperature distributions. It was desirable to reduce the diameter of the porous specimens to minimize the temperature differences. A 0.8-in. diameter specimen was considered the smallest practical size for the porous tungsten because of the depth of heating. However, subsequent experimental results showed less scatter with specimens 1.0 in. in diameter and larger.

The porous specimens were fabricated by gravity sintering tungsten particles 0.006 to 0.01 in. in size. The specimens were fired for a long duration at temperatures above 4000°F to achieve a stable mechanical structure. Attempts were made to use porous specimens fabricated from 0.02-in. particles, but the large particles did not sinter well which resulted in unsatisfactory mechanical strength.

The solid tungsten specimens were polished prior to use. However, continuous heating at high temperatures caused thermal etching of the surfaces. Consequently, the general surface condition for these specimens was a smooth finish with clearly defined grain boundaries.

The specimen was centered in the load coil, and the test chamber was evacuated to 10 microns Hg. A 30-minute heating period was maintained at each temperature level to insure steady-state conditions. Temperatures were measured on the top circular surface along the three radii shown in Fig. 5, at intervals of about 0.05 in. Two measurements were made at each location.

Typical sets of temperature distributions are shown in Figs. 6 and 7 for a solid and a porous tungsten specimen respectively. These temperatures, obtained with the optical pyrometer, have been corrected for the spectral emittance of the specimen, the transmissivity of the quartz window, and the reflectance of the front surfaced mirror. These corrections are discussed in Section 6. The temperature distribution is slightly asymmetric as shown by the temperature differences along the three radii. This skewing is caused by nonuniformities in the
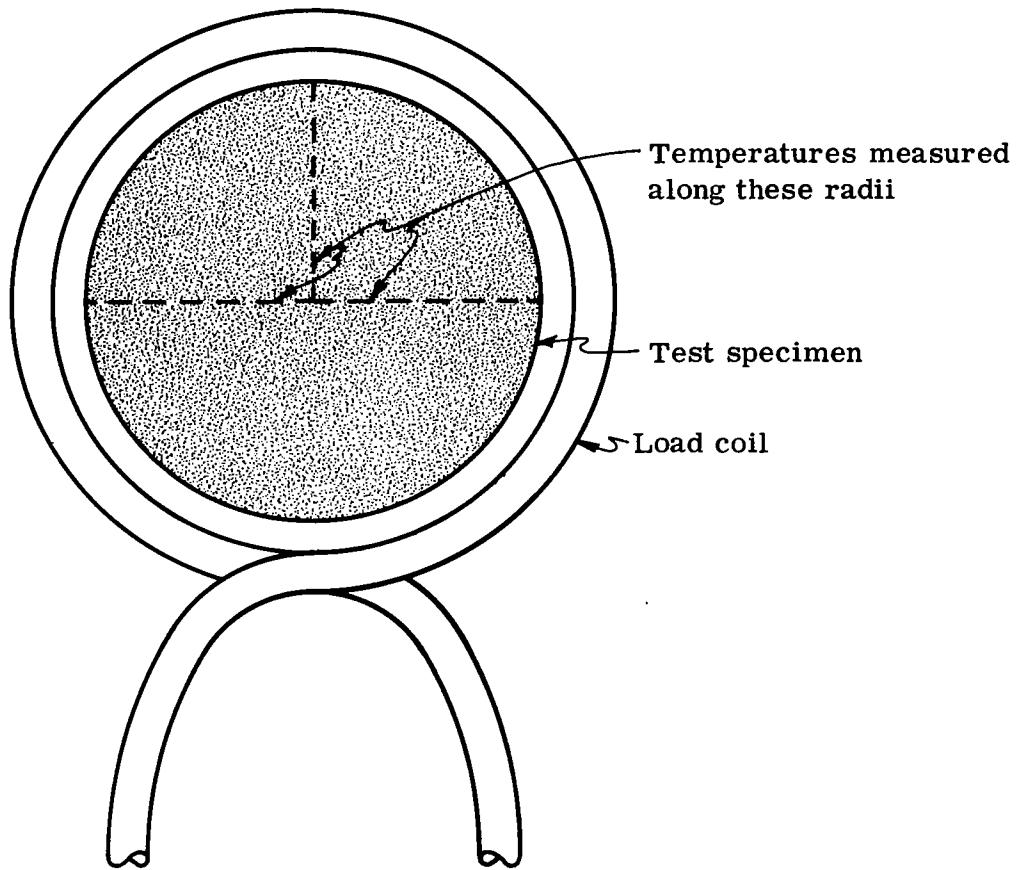
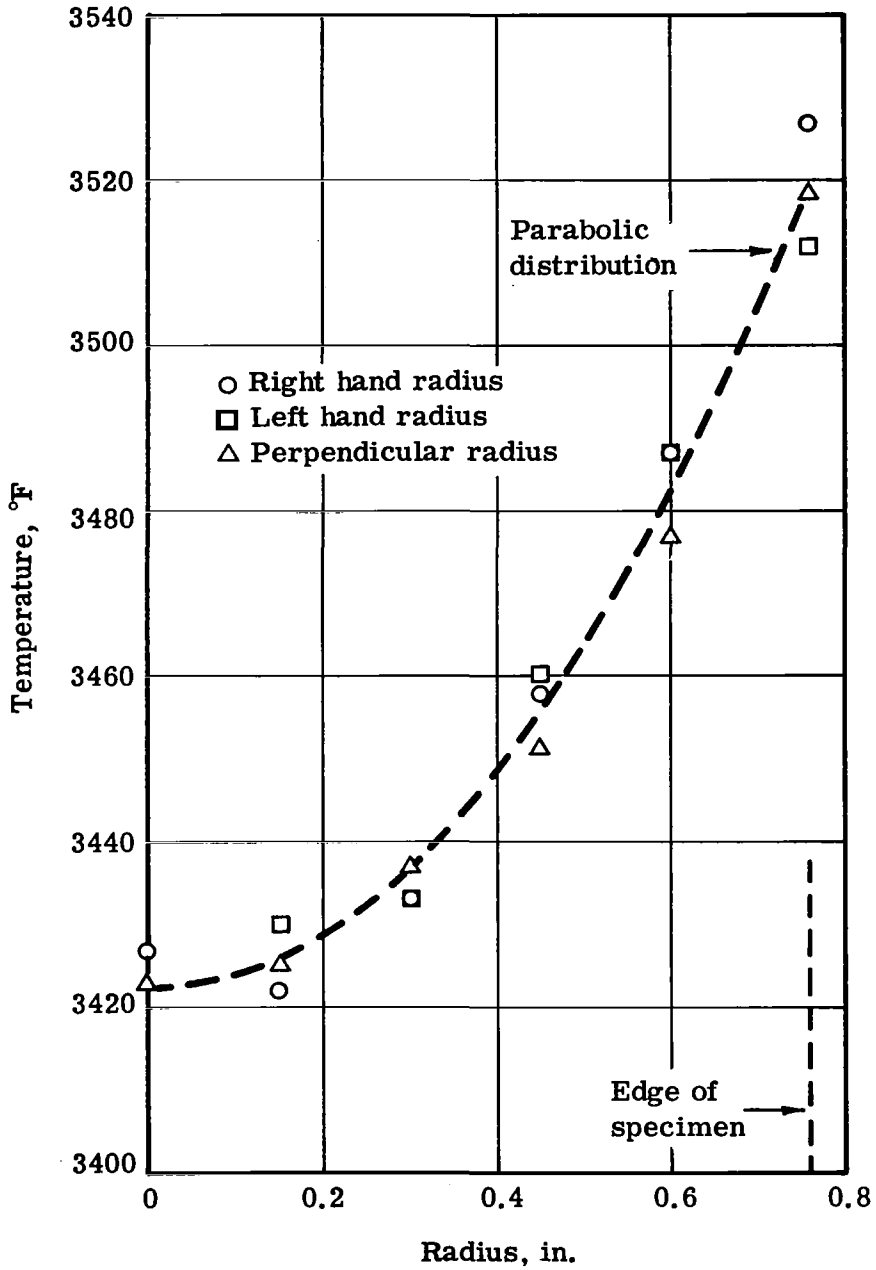Fig. 5 — Location of Temperature Measurements on Test Specimen

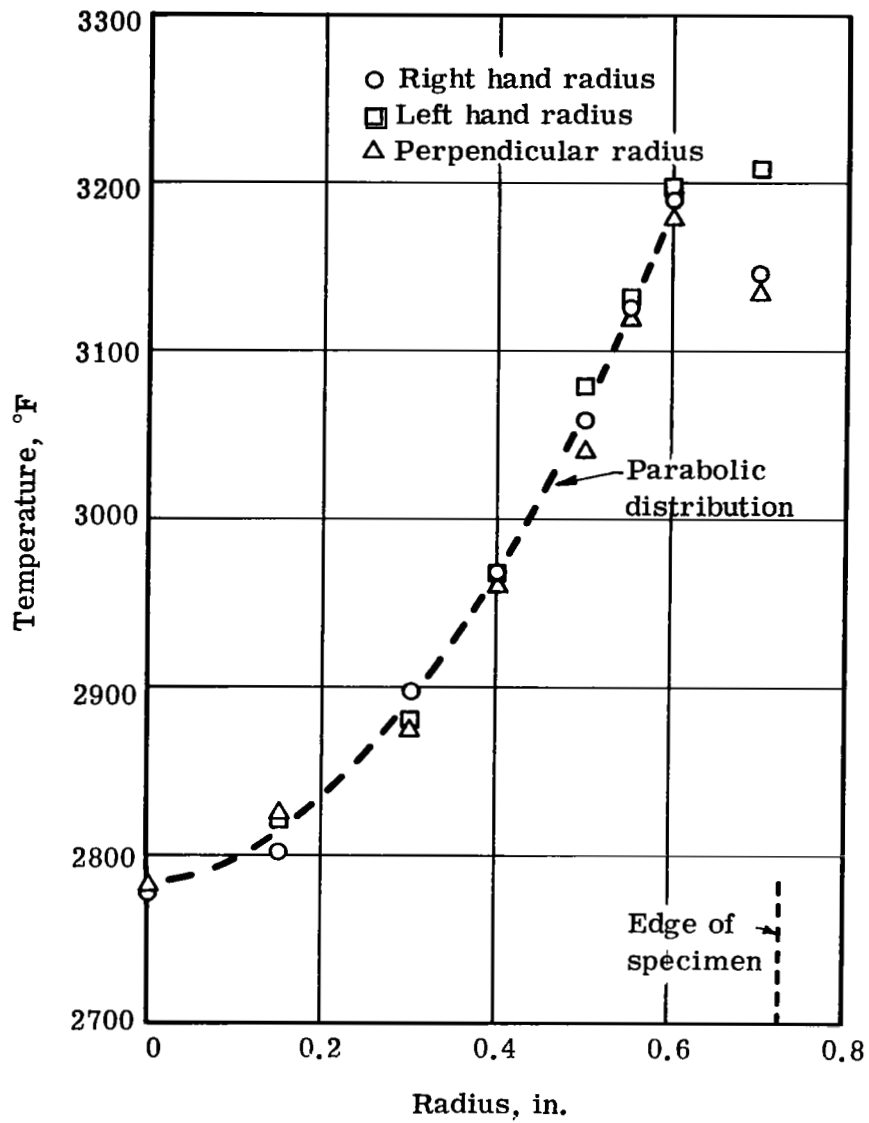Fig. 6 — Temperature Distribution for $1\frac{1}{2}$-in. Solid Tungsten Specimen (S1)

Fig. 7 — Temperature Distribution for $1\frac{1}{2}$-in. Porous Tungsten Specimen (P2)

induction heating process. In addition, there is some scatter in the temperatures at each radial location because of the subjective nature of making optical pyrometer measurements.

The temperature peaks at the outer edge with the solid tungsten specimens, but peaks about 0.1 in. from the edge with the porous tungsten specimens because of the larger depth of heating in the porous structure. A parabolic curve was fitted to each set of data by the method of least squares. Because the analysis showed that the parabolic distribution was applicable only in the pure conduction region, data taken in the outer 0.15 in. of the porous specimens were not used in fitting the curves.

Eq. 3 is used to determine the thermal conductivity of the specimens. The radial temperature difference on the upper surface is

$$T_{R,L} - T_{0,L} = C_1 R^2$$

and the proportionality factor, S_0, is

$$S_0 = C_2 \frac{L}{R}$$

Using these expressions in Eq. 3, the thermal conductivity of the specimens is

$$k = \frac{\epsilon_T \sigma T_{0,L}^4}{C_1 C_2 L} \tag{4}$$

where C_1 is the coefficient for the parabolic temperature distribution obtained from the least squares curve for each set of data. C_2 is the coefficient for the linear proportionality factor shown in Fig. 3. The total emittance, ϵ_T, is determined experimentally as described in Section 5.

The thermal conductivities calculated for the four solid tungsten specimens are shown in Fig. 8 as a function of average specimen temperature. The geometry of specimens had no determinable effect on the calculated values. The scatter (~20%) is attributed to the asymmetric temperature distributions observed on the top surface which are caused by nonuniformities in the induction heating.

The conductivities computed for the five porous tungsten specimens are shown in Fig. 9. Differences in the sintering of the specimens cause variations in the conductivity from one specimen to another even though they were fabricated from the same size particles. In Table 2, it can be observed that the porosity of the specimen does not have any definitive effect on the thermal conductivity. The 0.8-in. diameter specimen has the most scatter because the depth of heating in this specimen is relatively large compared to its diameter, and this makes it more sensitive to variations in the heating process.

TABLE 2 — POROUS TUNGSTEN THERMAL CONDUCTIVITY

Porosity	Thermal Conductivity, Btu/hr-ft-°F
0.55	5.2
0.45	11.4
0.46	10.2
0.42	8.2
0.42	9.8

There are two sources of errors which affect the values for thermal conductivities determined by this method.

1. Total hemispherical emittances, used in the thermal conductivity calculations, are averaged values over the temperature range of interest.
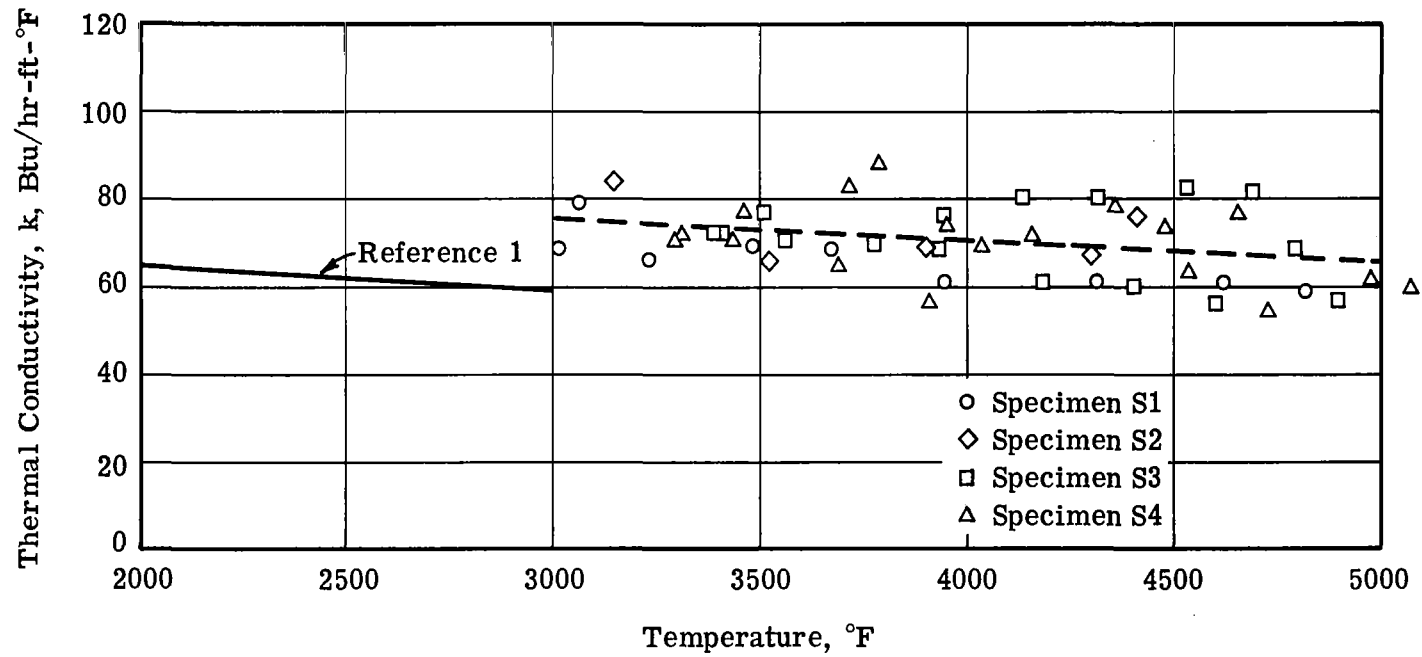
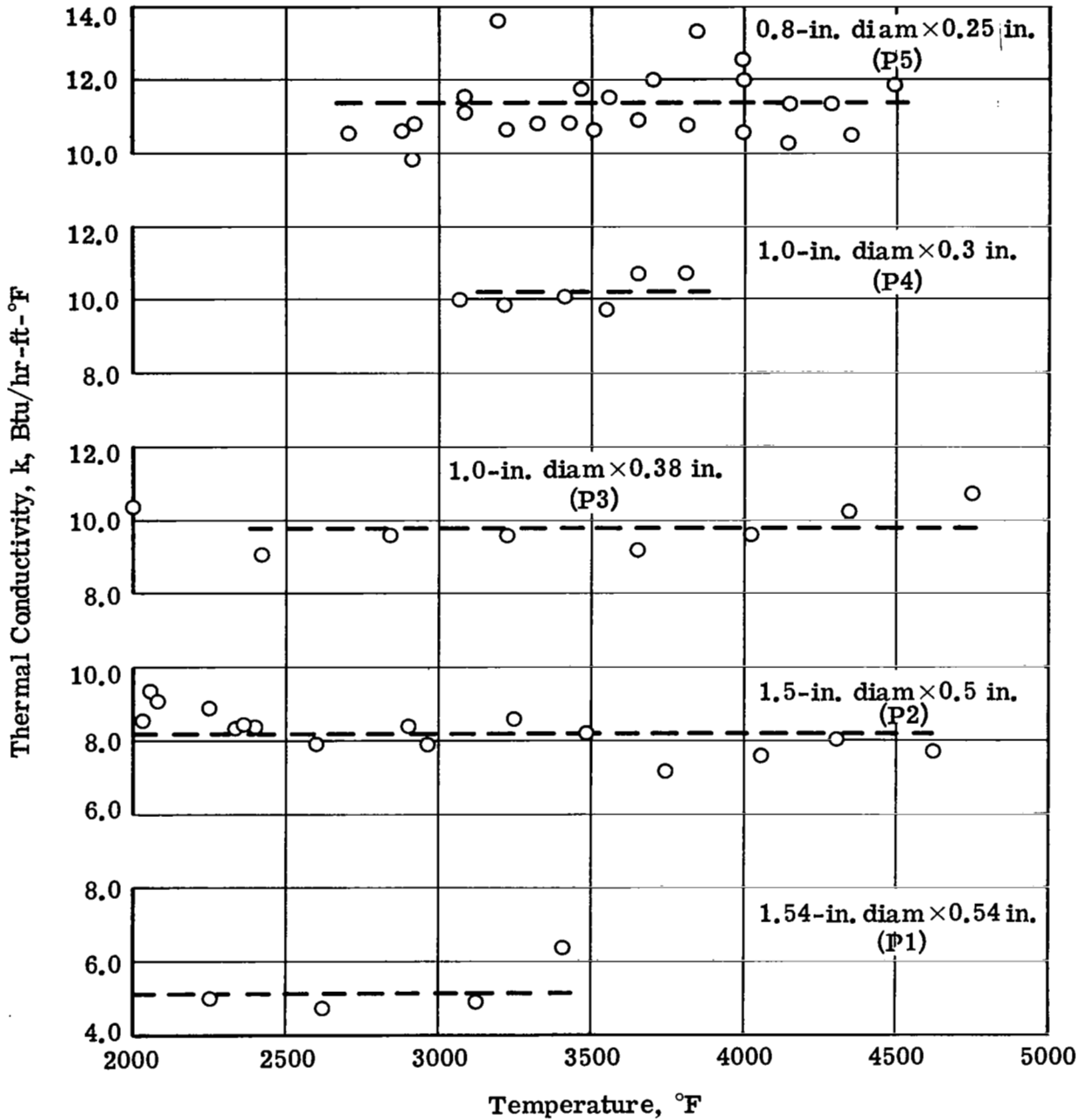Fig. 8 — Thermal Conductivity for Solid Tungsten

Fig. 9 — Thermal Conductivity of Porous Tungsten

2. There are inaccuracies in the results of the numerical solutions for the proportionality factor.

It is estimated that the averaged emittance values introduce a maximum uncertainty of 10% and inaccuracies in the proportionality factor contribute another 5% uncertainty in the calculated thermal conductivity values shown in Figs. 8 and 9.

The temperature distributions obtained in the experimental program are presented in Reference 5.

5. TOTAL EMITTANCE MEASUREMENTS

Total normal and total hemispherical emittances were measured for solid and porous tungsten specimens similar to those used in the conductivity experiments. These measurements were made with a total radiation pyrometer that was mounted above the test chamber and focused on the center of the top surface of the specimen.

5.1 TOTAL NORMAL EMITTANCE

The pyrometer was calibrated with a black body source that was heated in the test chamber in an argon atmosphere. This black body source consisted of a 0.3-in. diameter $\times$ 1.5-in. hole in the center of a 0.75-in. diameter $\times$ 1.75-in. graphite rod. The rod was wrapped with five layers of tungsten foil radiation shields. The output of the radiation pyrometer, which was focused on the black body hole, was recorded at different temperature levels between 2000 and 4300°F. The emf output from the pyrometer, corrected for the long wave cutoff of the quartz window, was proportional to the radiation heat flux. Thus, the total normal emittance of the tungsten specimens can be determined from the ratio of the measured emf's.

$$\epsilon_{TN} = \frac{(emf)_{specimen}}{(emf)_{black\ body}} \ .$$

Total normal emittances were measured in vacuum for three solid tungsten specimens and one porous tungsten specimen. The three solid tungsten specimens

were used to evaluate any variations in the effects of thermal etching on normal emittance values. Slight variations in surface condition are not an important factor for the porous tungsten because of the coarse texture of the specimen surface. The measured emittances for solid and porous tungsten are shown in Figs. 10 and 11 respectively. The solid emittances show small differences among the specimens examined, indicating a slight surface finish effect on the values measured. These values are approximately 10% higher than published normal emittances for polished tungsten. This difference is attributed to the etched finish. There are no published data for porous tungsten normal emittances that can be compared with the values shown in Fig. 11.

5.2 TOTAL HEMISPHERICAL EMITTANCE

The method used to determine the total hemispherical emittances was first proposed by Hoch.[4] This technique relates the sensible heat loss from the specimen during cooldown to the heat loss radiated from the specimen surface,

$$\frac{dQ}{d\tau} = - \int \epsilon_T \sigma T_s^4 \, dA$$

The specific heat of tungsten varies linearly with the temperature as shown in Reference 6.

$$C_p = k_1 + k_2 T$$

Using this expression, the heat stored in the specimen is

$$Q = \int \rho (k_1 + k_2 T) T dV \approx \rho V (k_1 + k_2 \overline{T}) \, \overline{T}$$

where $\overline{T}$ is the volume averaged temperature of the specimen. Similarly, the radiation term is defined as

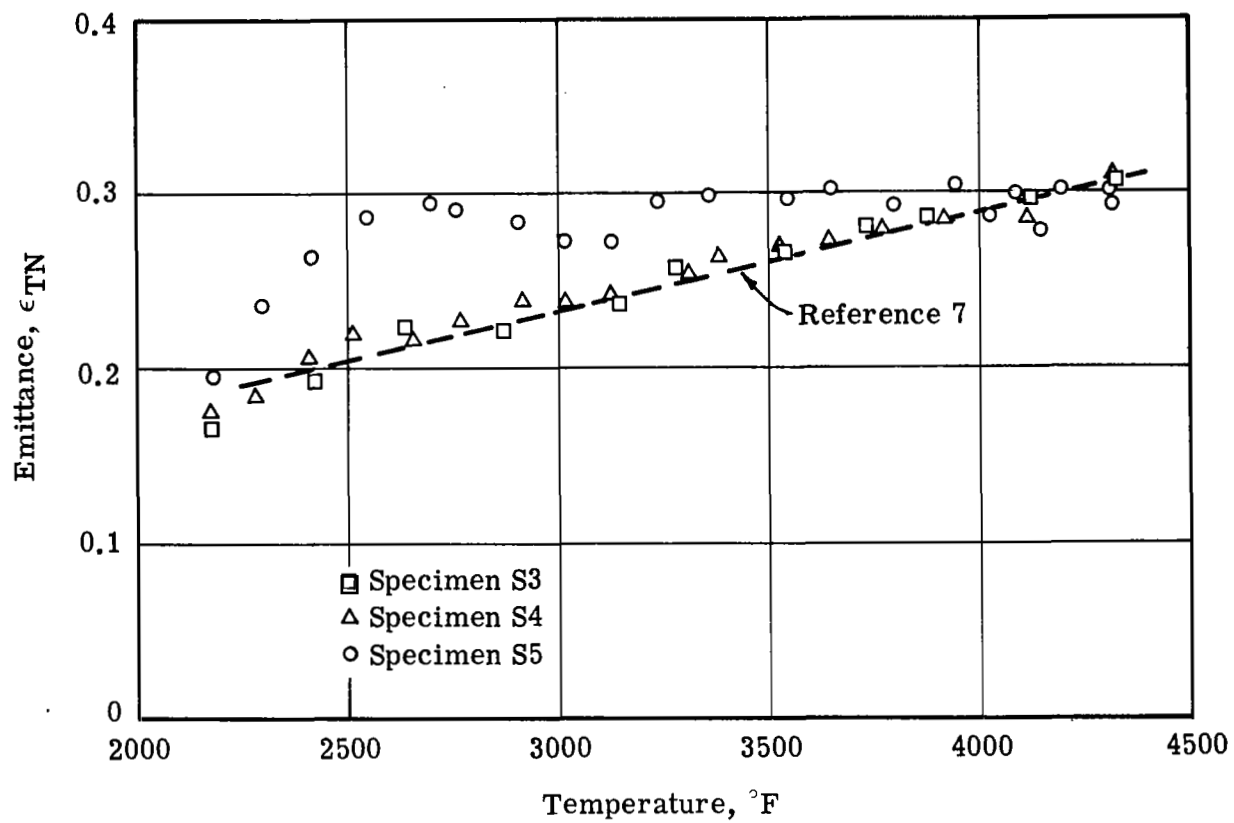$$- \int \epsilon_T \sigma T_s^4 \, dA = -\epsilon_T \sigma A \overline{T}_s^4$$

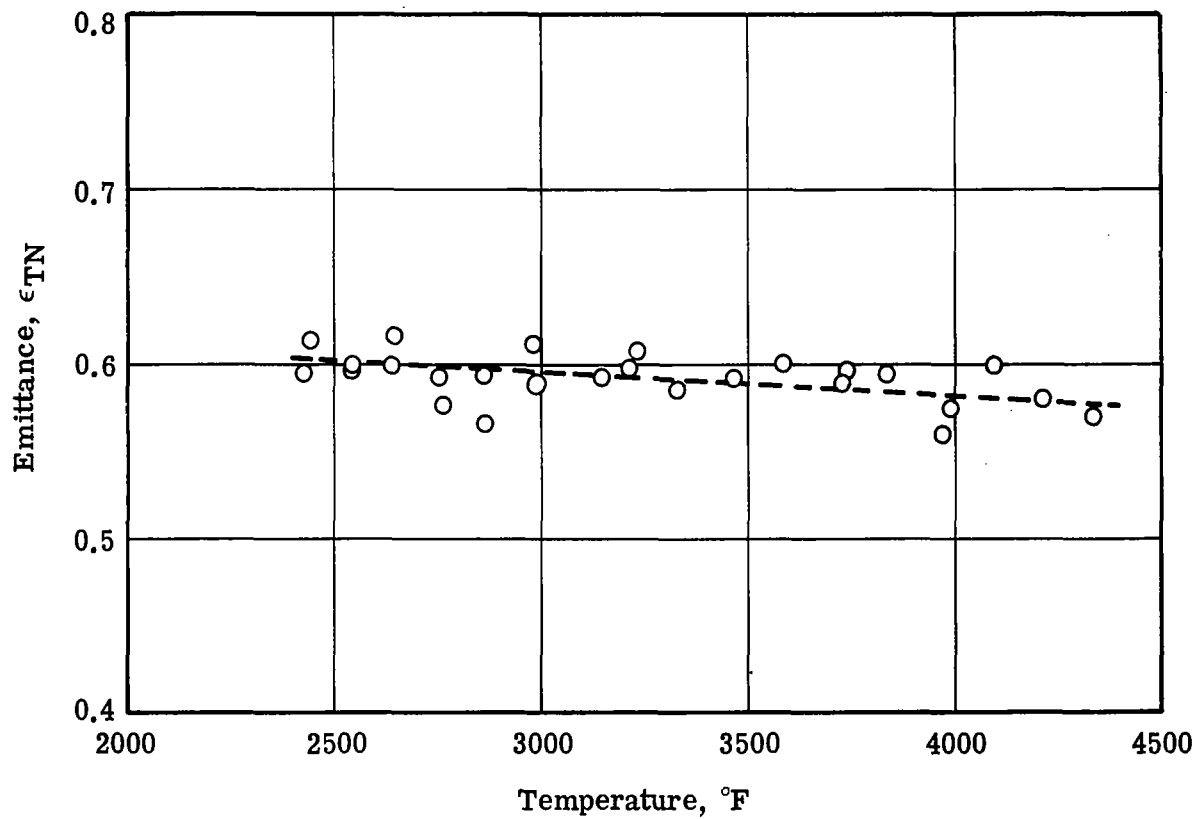Fig. 10 — Total Normal Emittance for Solid Tungsten

Fig. 11 — Total Normal Emittance for Porous Tungsten

where $\overline{T}_S$ is the averaged surface temperature. The total hemispherical emittance is assumed to be constant. A heat balance results in the following equation:

$$\frac{d[\rho V(k_1 + k_2\overline{T})\overline{T}]}{d\tau} = -\epsilon_T \sigma A T_S^4 .$$

Because only the top center temperature is recorded during cooldown, a functional relationship must be obtained relating the measured temperature, T_C, to the average specimen and surface temperatures, $\overline{T}$ and $\overline{T}_S$.

A solution to the transient temperature distribution in porous and solid tungsten specimens during cooldown was obtained with a computer code similar to the one used to determine the steady-state temperature distributions. The results showed that the temperatures in the solid tungsten specimen were nearly uniform after the first two seconds of the transient period. Therefore,

$$\overline{T} \approx \overline{T}_S \approx T_C.$$

However, the results for the 0.8-in. diameter $\times$ 0.4-in. porous tungsten specimen showed the average surface temperature was appreciably lower than the top center temperature during cooldown, while the average specimen temperature was nearly the same. The computer solutions result in the following temperature relations for the porous specimen.

$$\overline{T} \approx T_C$$

$$\overline{T}_S = k_3 T_C^{k_4}$$

Using these temperature relationships, the heat balance equation can be integrated to form

$$k_S + \epsilon_T \tau = \left[\frac{\rho V}{\sigma A k_3^4} \left(\frac{k_1}{4k_4 - 1} \times \frac{1}{T_C^{4k_4 - 1}} + \frac{2k_2}{4k_4 - 2} \times \frac{1}{T_C^{4k_4 - 2}} \right) \right] \qquad (5)$$

where k_S is the integration constant.

The data during cooldown were obtained with a millivolt recorder attached to the total radiation pyrometer. The pyrometer output was calibrated against temperature during the heatup of the specimen. The specimens were cooled down from different temperature levels to permit using maximum recorder spans over the different temperature ranges.

The total hemispherical emittance values were determined by a least squares fit of the cooldown transient data to Eq. 5. Because of the uncertainty in these published data, the specific heat was adjusted to make the hemispherical and normal emittances equal for the porous specimen. This is a reasonable approximation for rough surfaces. The value of specific heat thus obtained was then used to calculate the hemispherical emittance of the solid tungsten.

The total hemispherical emittances for solid and porous tungsten are shown in Fig. 12. Values for the solid tungsten are higher than the measured normal emittances. This agrees with data presented in Reference 7. This difference is attributed to the fact that tungsten does not obey Lambert's cosine radiation law.[8] Published total hemispherical emittances for polished solid tungsten show a slight temperature dependence in this range.

The hemispherical emittances shown in Fig. 12 represent average values over the temperature range of interest. This is because the data do not permit the calculation of emittances over small temperate spans.
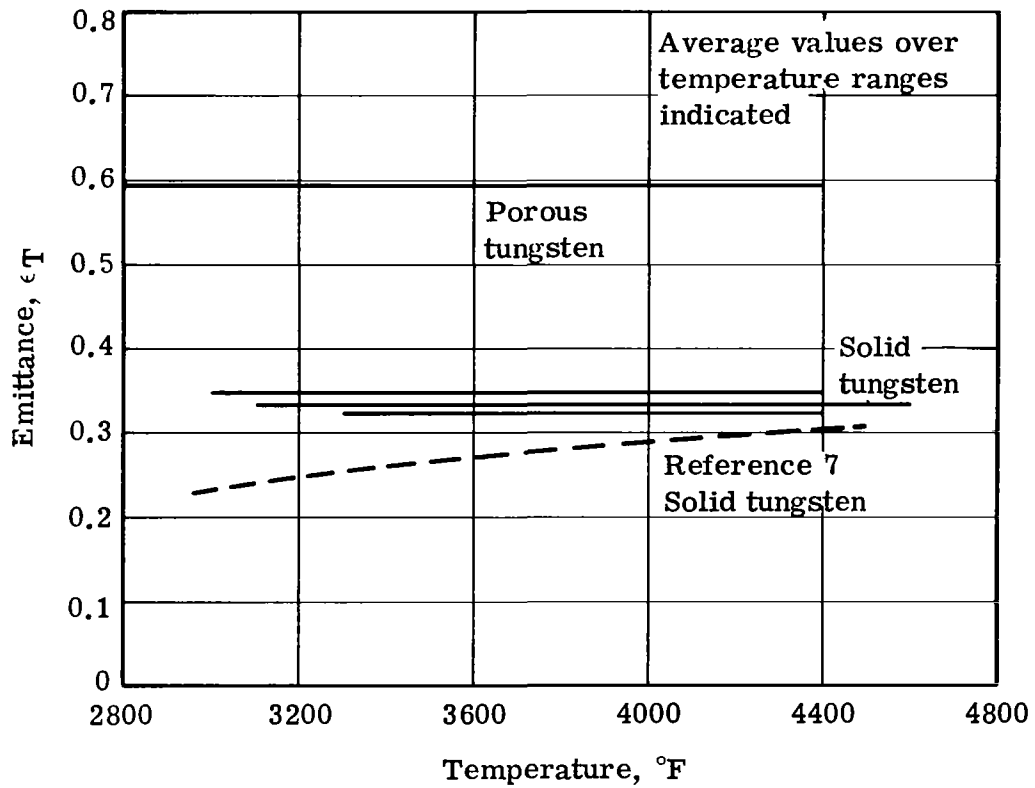
Fig. 12 — Total Hemispherical Emittance for Solid and Porous Tungsten

6. SPECTRAL EMITTANCE MEASUREMENTS

Spectral emittances were measured for tungsten using porous and solid specimens with central black body holes. The spectral emittances were determined from observed temperatures in the black body holes and temperatures of the surface adjacent to the hole.

The radiant energy flux of a nonblack body is obtained from Wien's formula

$$J = \epsilon_\lambda C_1 \lambda^{-5} e^{-C_2/\lambda T_T} \tag{6}$$

where T_T is the actual temperature of the body and ϵ_λ is its spectral emittance. Since the optical pyrometer is calibrated for a black body, the temperature recorded with the pyrometer is the brightness temperature, T_{br}, and is related to the energy flux as

$$J = C_1 \lambda^{-5} e^{-C_2/\lambda T_{br}} \tag{7}$$

However, the radiant energy fluxes given in Eqs. 6 and 7 are equivalent. Therefore, the spectral emittance can be evaluated by equating the above equations:

$$\ln \epsilon_\lambda = \frac{C_2}{\lambda} \left(\frac{1}{T_T} - \frac{1}{T_{br}} \right)$$

This procedure can be reversed when reducing the data to determine the actual specimen temperature from the observed values and the spectral emittances.

Spectral emittances for solid tungsten were determined using a 0.5-in. diameter ×
0.5-in. high specimen containing a central black body hole 0.02-in. diameter ×
0.25-in. deep. Measurements were made for both polished and thermally etched
specimen surfaces in vacuum. The etched surface corresponded to the surface
finish of the solid specimens used in the thermal conductivity experiments. In
addition, measurements were made with a polished surface in a hydrogen atmos-
phere.

The spectral emittances calculated for solid tungsten are shown in Figs. 13, 14,
and 15. The specimen surface condition and the atmosphere have little effect on
spectral emittance values. The absolute values of these emittances are approxi-
mately 10% higher than values given in Reference 7 for the temperature range of
interest.

A specimen 0.6-in. diameter × 0.3-in. high, having a 0.02-in. diameter × 0.08-in.
deep central black body hole, was used for the spectral emittance measurements
on porous tungsten. This specimen was fabricated in the same fashion as those
used for the thermal conductivity measurements. The surface of the porous spec-
imen, when viewed through the optical pyrometer, had a mottled appearance be-
cause of the difference in effective emittance between the grains and the pores.
In making optical pyrometer measurements on the porous specimens, the temper-
atures were always obtained by matching the pyrometer filament to the pore
brightness.

The spectral emittances, measured for porous tungsten in vacuum and a hydrogen
atmosphere, are shown in Figs. 16 and 17. The difference in values shown is
probably caused by optical distortions created by natural convection currents in
the hydrogen atmosphere.

Similar measurements were made to determine the transmissivity of the quartz
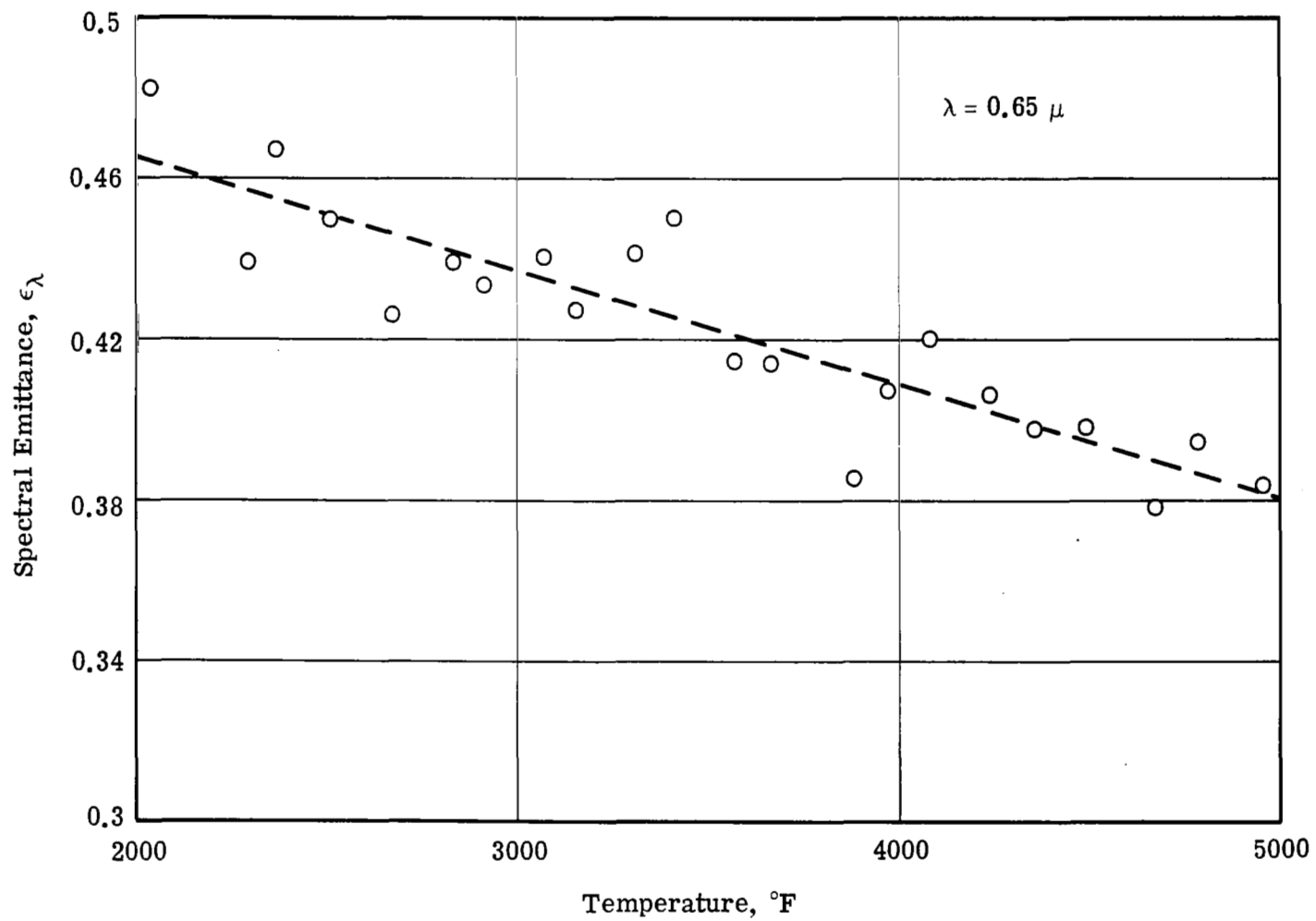windows and the reflectivity of the front surfaced mirror. Instead of using a

34

Fig. 13 — Spectral Emittance for Solid Tungsten – Vacuum Atmosphere
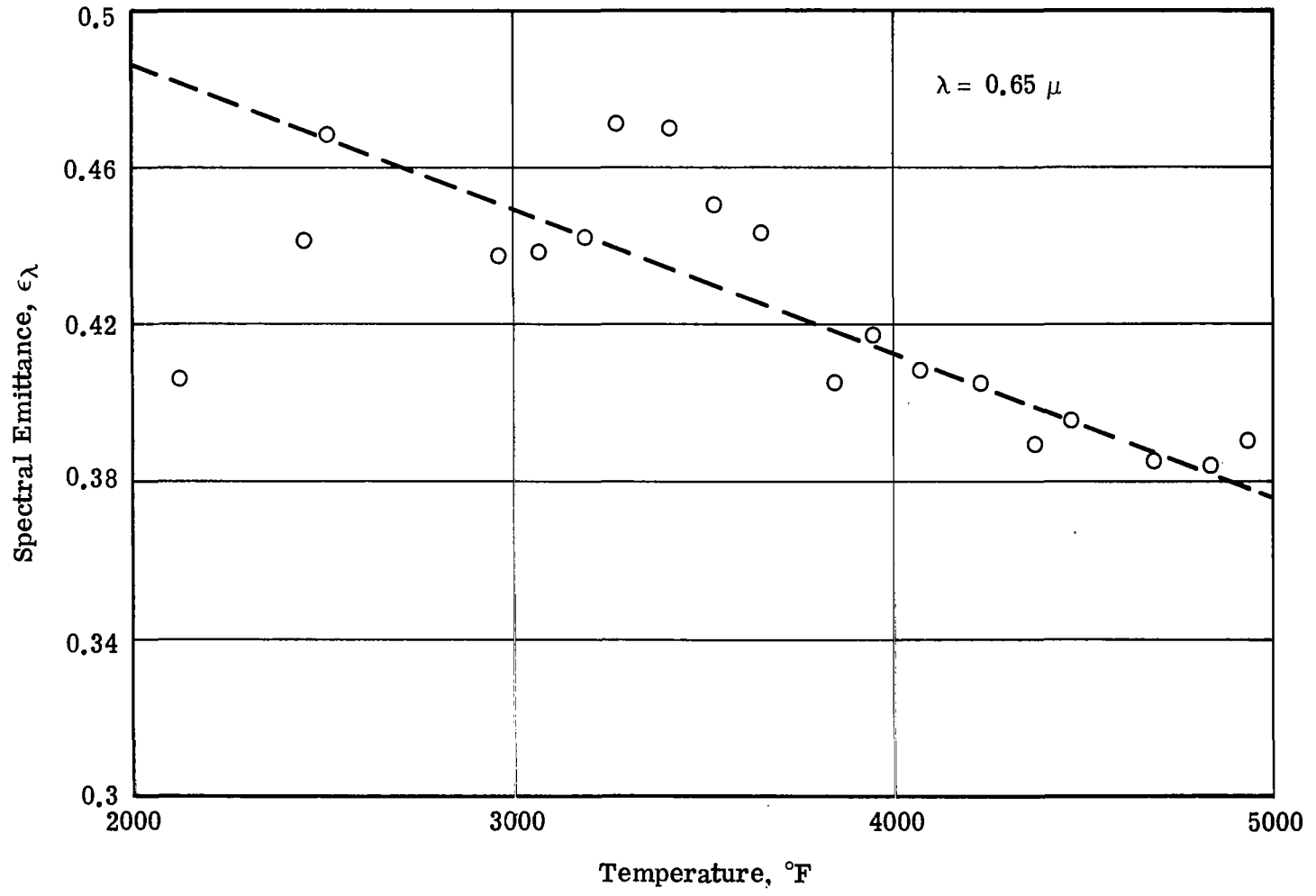Polished Surface

Fig. 14 — Spectral Emittance for Solid Tungsten — Vacuum Atmosphere
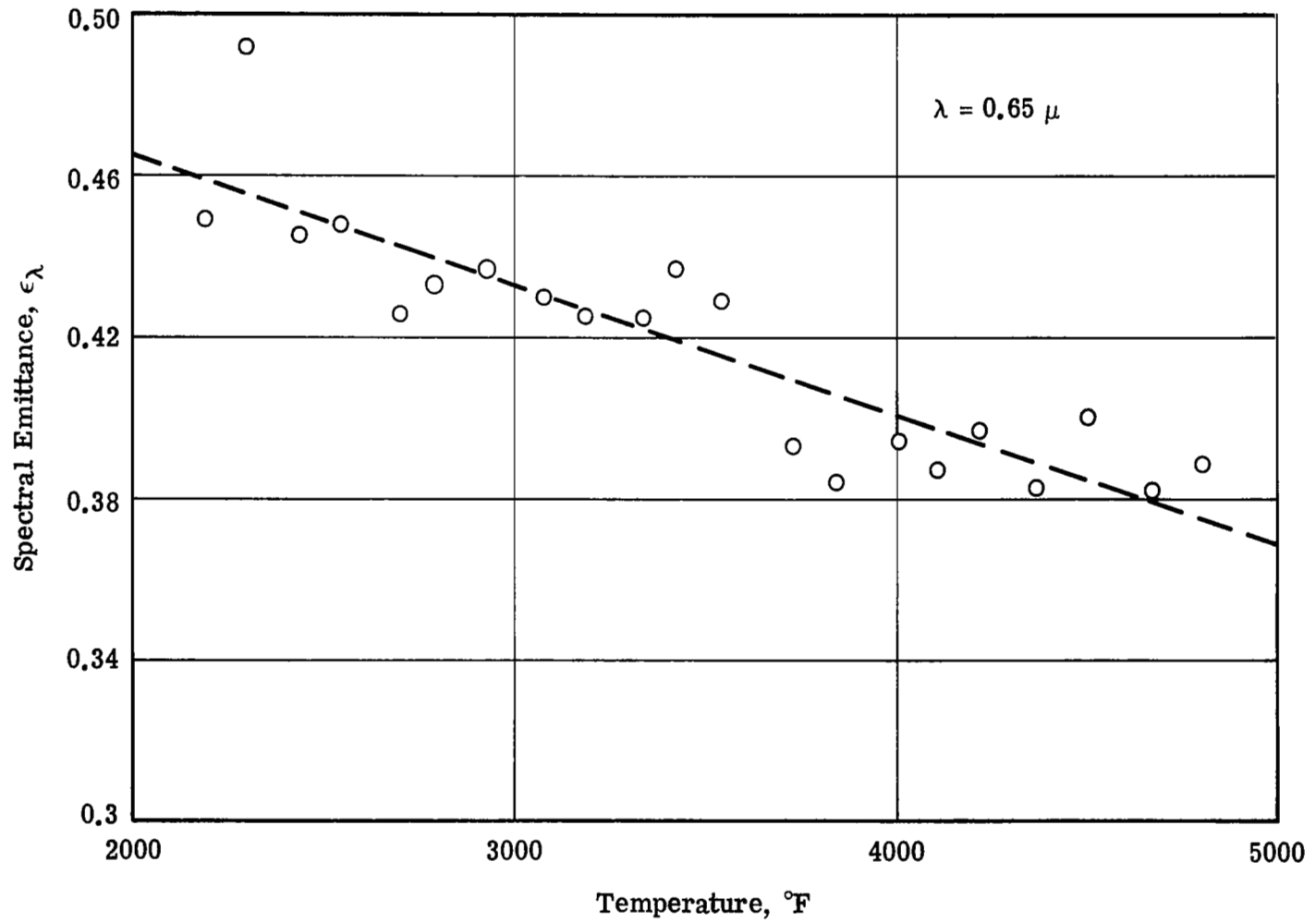Etched Surface

Fig. 15 — Spectral Emittance for Solid Tungsten – Hydrogen Atmosphere
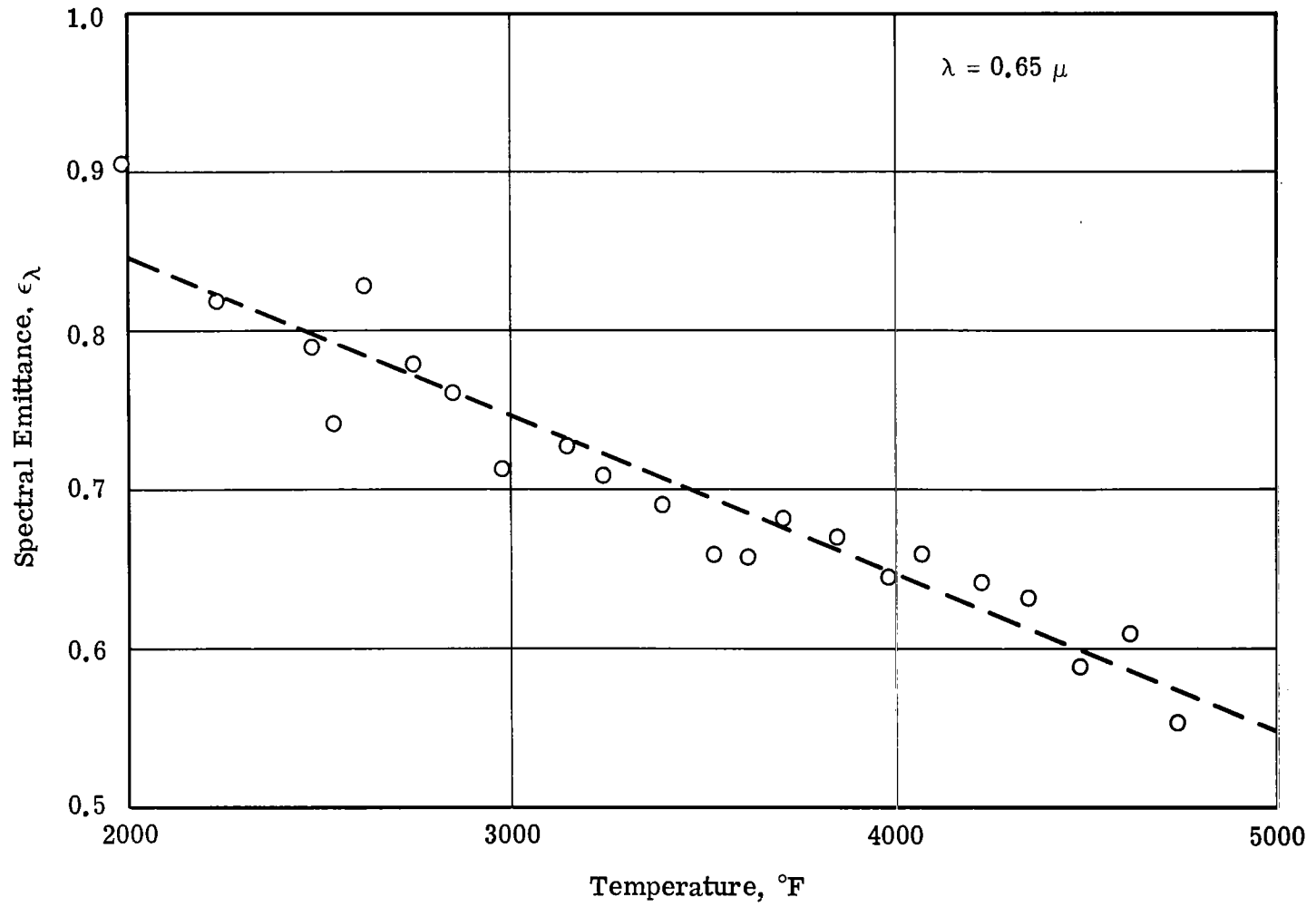Polished Surface

Fig. 16 — Spectral Emittance for Porous Tungsten — Vacuum Atmosphere
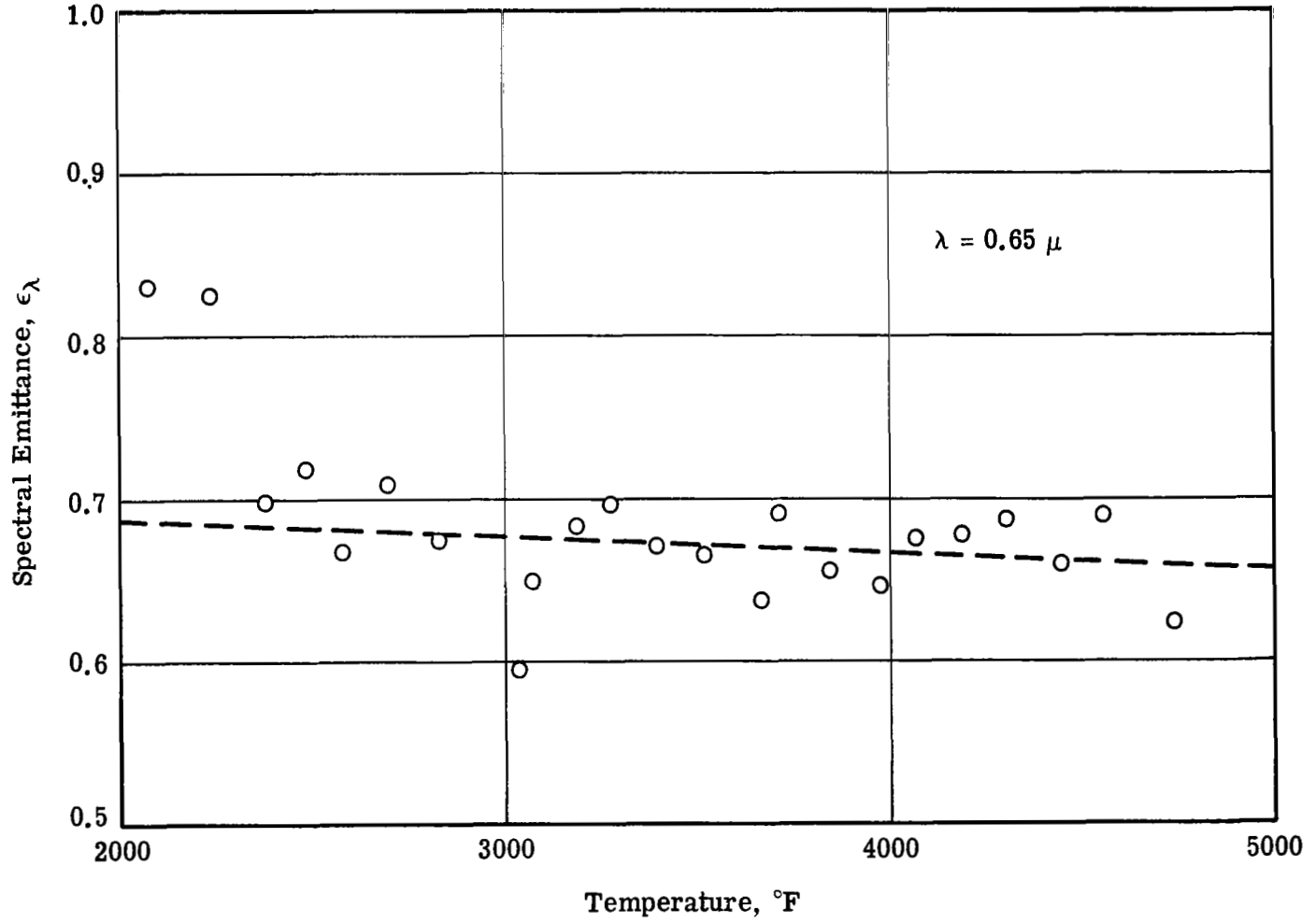Measured at Pores on Surface — Particle Size, 0.008 to 0.010 in.

Fig. 17 — Spectral Emittance for Porous Tungsten — Hydrogen Atmosphere
Measured at Pores on Surface — Particle Size, 0.008 to 0.010 in.

black body hole, temperature measurements at a fixed point were made with and without these optical components in place and the data were reduced with Wien's formula. The reflectivity of the mirror is 0.81 and the transmissivity of the quartz windows is 0.92.

7. NOMENCLATURE

A   Surface area

C_p Specific heat

J   Radiant energy flux

k   Thermal conductivity

L   Half height of specimen

Q_0 Heat generation source term

r,R   Radial dimension

S_0 Proportionality factor

T   Temperature

V   Volume

z   Axial dimension

ϵ_λ Spectral emittance

ϵ_T Total hemispherical emittance

ϵ_{TN} Total normal emittance

λ Wave length

ρ Density

σ Stefan-Boltzmann constant

τ Time variable

8. REFERENCES

1. Goldsmith, A., Waterman, T., and Hirschhorn, H.: "Handbook of Thermophysical Properties of Solid Materials," Vol. 1, Elements (Melting Temperature above 1000°F), Pergamon Press, New York, 1961.

2. Israel, S., Hawkins, T., and Hyman, S.: Thermal Conductivity of Hydrogen from 2000°F to 4700°F, NASA CR-403, 1966.

3. Hoch, M. and Nitti, D.: New Method for the Determination of Thermal Conductivities between 1000° and 3000°C, ASD-TR-61-528 (June 1962).

4. Hoch, M. and Narasimhamurty, H.: Relation between Specific Heat and Emissivity of Tantalum at Elevated Temperatures, ASD-TDR-63-371 (July 1963).

5. Israel, S., Hawkins, T., and Hyman, S.: Experimental Data for the Effective Thermal Conductivity of Solid and Porous Tungsten in Vacuum and Hydrogen Atmospheres, NASA CR-54429 (Aug. 1965).

6. Lowenthal, G., The Specific Heat of Metals between 1200°K and 2400°K, Aust. J. of Phys., 16:1 (Mar. 1963).

7. Wood, A., Beem, H., and Lucks, C.: The Emittance of Chromium, Columbium, Molybdenum, Tantalum, and Tungsten, DMIC Memorandum 141 (Dec. 1961).

8. Larrabee, R.: The Spectral Emissivity and Optical Properties of Tungsten, MIT-TR-328 (May 1957).

9. APPENDIX – EQUATIONS USED IN NUMERICAL SOLUTION OF BOUNDARY VALUE PROBLEM

One-quarter of the cross section of the cylinder is used to analyze the temperature distribution within the specimen because of symmetry about the axis and the midplane. The geometry is divided into 20 to 30 radial nodes and 10 to 15 axial nodes. The axial nodes are of uniform size. The radial nodes in the heat generating region at the outer edge of the specimen are smaller than the radial nodes in the pure conduction region. Temperatures are determined at the center of each node and at the center of the boundary node outer surfaces.

The steady-state temperature distribution in the specimen is determined by satisfying the local heat balances for all nodes simultaneously. The heat balance for each node is

$$Q_0 = \sum_{n=1}^{4} (T_0 - T_n) Y_n$$

where $Q_0 \equiv$ heat generation in node (0)

$T_0 \equiv$ center temperature of node (0)

$T_n \equiv$ center temperature of node (n)

$Y_n \equiv$ heat transfer coefficient between adjacent nodes (n and 0) based on the temperature difference between the centers of the nodes.

43

The above equation is used for each node to determine the change in its center temperature at each iteration as,

$$\Delta T_0 = \frac{Q_0 + \sum\limits_{n=1}^{4} T_n Y_n}{\sum\limits_{n=1}^{4} Y_n} - T_0$$

The solution for each problem is completed when the calculated temperature change, ΔT, for every node is less than $0.05°F$. To speed convergence, the temperature change at each iteration is calculated by $\omega(\Delta T)$ where ω is an overrelaxation factor equal to 1.8.

The heat transfer coefficients between nodes are determined by the geometry and thermal conductivity. Referring to Fig. 18, the axial heat transfer coefficient between nodes 1 and 2 is:

$$Y_{1-2} = \frac{\pi k (r_2^2 - r_1^2)}{\Delta z}$$

The radial heat transfer coefficients are calculated by

$$Y_{1-3} = \frac{2\pi k \Delta z}{\ln \dfrac{r_3 + r_2}{r_2 + r_1}}$$

The heat transfer coefficient at the surface accounts for radiation to an infinite media at zero temperature. It is

$$Y_S = \epsilon_T \sigma A T_S^3$$

where A = the surface area
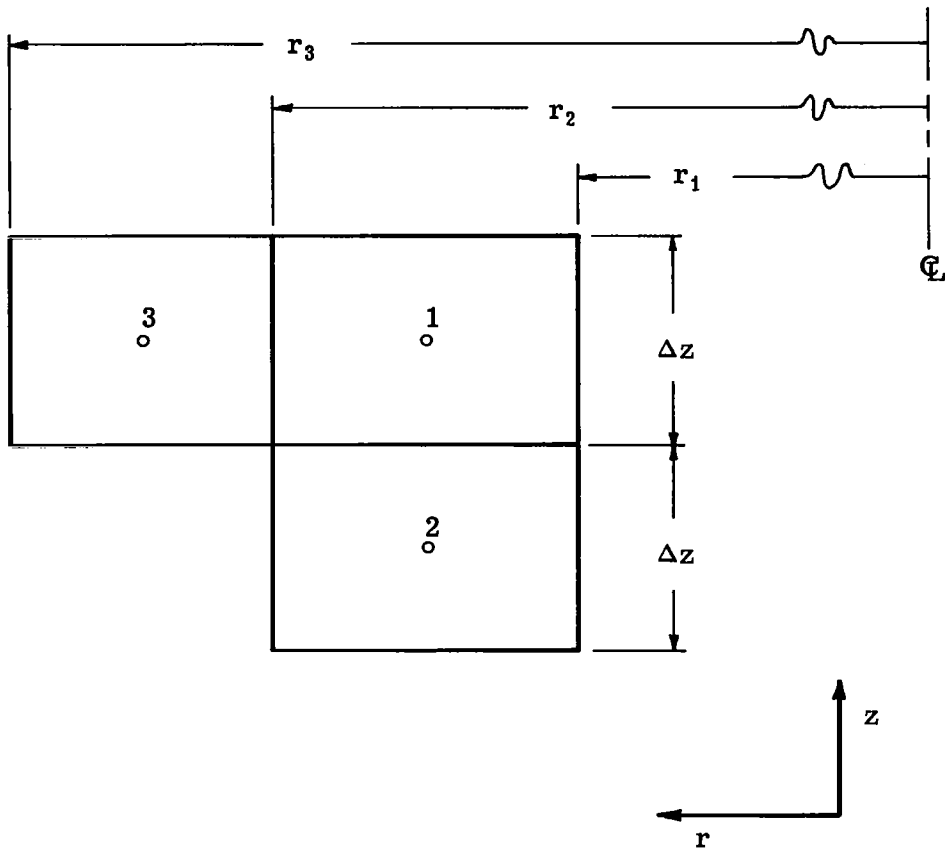
T_S = the surface temperature.

44

Fig. 18 — Nodal Geometry

The errors introduced by the numerical solution are estimated to be about 5%.

Similar equations are used to determine the transient temperature distribution during cooldown of the specimen. Instead of using relaxation to determine the temperatures at each iteration, the first forward difference method is used to calculate the temperature changes at each time interval, as

$$T_0' = \frac{Q_0 - \sum\limits_{n=1}^{4} (T_0 - T_n) Y_n}{\rho V_0 C_p} \times \Delta\tau + T_0 \ .$$